Design of millimeter-wave detectors based on zero-bias Schottky diode for direct detection system of CubeSat radiometer

CHEN Yao[1,2]， ZHANG Sheng-Wei[1*]

（1. Key Laboratory of Microwave Remote Sensing，National Space Science Center，Chinese Academy of Sciences，
Beijing 100190，China；

2. University of Chinese Academy of Sciences，Beijing 100049，China）

Abstract：In this paper，two millimeter-wave zero-bias Schottky detectors for the direct detection system of the CubeSat radiometer，with center frequencies of 89 GHz and 150 GHz，respectively，were designed and implemented. These designs were based on zero-bias Schottky diodes of ACST. A radial stub structure was adopted at the DC ground and output port with a tuning line for optimum impedance matching to achieve stable and high performance and broadband characteristics；this structure also makes the circuit easier to integrate with pre-level systems and more suitable for CubeSat radiometer miniaturization. Circuit structure and Schottky diode were analyzed，modeled，and optimized to obtain better performance. The results showed that the W-band detector has a typical sensitivity of about 2500 V/W in the range of 85 GHz to 95 GHz and a linearity of 0. 9994 at 89 GHz. Moreover，the D-band detector has a typical sensitivity of about 1600 V/W in the range of 145 GHz to 155 GHz and a linearity of 0. 9992 at 150 GHz. These results verified the advantages of the improved circuit structure in the detector and the feasibility of the direct detection system.

Key words：millimeter-wave，detector，zero-bias Schottky diode，impedance matching

基于立方星辐射计直接检波系统的毫米波零偏置肖特基二极管检波器设计

陈　峣[1,2]， 张升伟[1*]

（1. 中国科学院国家空间科学中心，中国科学院微波遥感技术重点实验室，北京 100190；

2. 中国科学院大学，北京 100049）

摘要：基于立方星辐射计直接检波系统，设计并实现了中心频率分别为 89 GHz 和 150 GHz 的两款毫米波零偏置肖特基检波器。检波器设计基于 ACST 的零偏置肖特基二极管。为了获得稳定、优越的性能以及较好的宽带特性，并易于与前级系统集成，更适于立方星辐射小型化，在直流接地电路与输出电路处采用扇形线结构，并通过一段可调传输线对其端口阻抗进行优化。本文对肖特基二极管及检波器电路结构进行了分析、建模和优化。测试结果表明，W 波段检波器在 85～95 GHz 范围内具有 2500 V/W 的典型灵敏度，在 89 GHz 测试的线性度为 0.9994。D 波段检波器在 145～155 GHz 范围内的典型灵敏度约为 1600 V/W，在 150 GHz 测试的线性度为 0.9992。这些结果验证了改进电路结构在检波器设计上的优越性和在直接检波系统中应用的可行性。

关　键　词：毫米波；检波器；零偏置肖特基二极管；阻抗匹配

中图分类号：TN454；TN763.1　　　　　　　　　　**文献标识码**：A

Introduction

The CubeSat radiometer technology developed rapid-ly in recent years to meet the requirements of extreme weather observations[1-4]. In this work，89 GHz and 150 GHz are selected as window area detection frequencies.

Meanwhile, in order to reduce the volume, mass, and total power consumption of the radiometer, these two channels adopt the direct detection mode.

Zero-bias Schottky detectors are very mature in America and European countries. In 2014, Hoefle and Penirschke et al. [5] designed an 89 GHz zero-bias detector for the direct detection system of the European Meteorological Satellite program, which was applied in MetOp-SG. The voltage sensitivity of the detector is higher than 860 V/W (before amplification). Tekbaş et al. [6] designed a W-band detector based on the zero-bias Schottky diode using the antipodal finline transition structure. The voltage sensitivity is above 500 V/W over 85 GHz to 110 GHz. In China, Zhang et al. [7] developed a 270 GHz detector based on a typical circuit structure, and the voltage responsivity in the range of 260 ~280 GHz was greater than 1200 V/W. Meanwhile, Zhang et al. [8] designed a W-band detector based on the VDI zero-bias Schottky diode using the antipodal finline transition structure. The voltage sensitivity is above 2000 V/W over 86 GHz to 94 GHz. Yao et al. [9] developed two detectors: one in the W-band and the other in the D-band. The sensitivity of the W-band detector is higher than 2000 V/W from 80 GHz to 104 GHz, and the typical sensitivity of the D-band detector is 600 V/W in the range of 110 ~170 GHz. However, these detector circuits based on the typical structure or antipodal finline transition structure are not suitable for circuit integration or CubeSat radiometer miniaturization because they are not compact enough.

In this paper, two millimeter-wave detectors were developed with center frequencies of 89 GHz and 150 GHz, respectively. The detectors were designed based on the zero-bias Schottky diode from ACST[10] in which 3DSF30 was used in the W-band detector and 3DSF20 was used in the D-band detector. Both Schottky diodes are 147 μm long, 46 μm wide, and 7.5 μm thick. According to the requirements of CubeSat radiometer miniaturization, the zero-bias Schottky diode detector circuit structure was improved. A radial stub structure was applied to replace the traditional low-pass filter (LPF) RF short end, which reduced the length of the whole circuit and made it more compact. Meanwhile, by paralleling the DC ground port and DC output port with a radial stub, the effects of external loads connected to the ground or output port on module performance were reduced, and the stability of the detector was improved. A tuning line was connected to the radial stub to adjust its impedance for optimum impedance matching. In addition, we changed the position of the DC ground port to facilitate circuit integration and CubeSat radiometer miniaturization.

1 Design of Millimeter-wave Detector

The zero-bias waveguide detector generally contains a waveguide transition, matching network, Schottky diode, LPF, and other transmission structures[5-9]. When the DC bias voltage is V_0, the DC bias current is I_0, and a small AC voltage δV is loaded on both ends of the Schottky diode. $i(V)$ can be obtained by using Taylor se-

ries expansion:

$$i(V) = i(V_0) + \delta V \left.\frac{di}{dv}\right|_{I_0} + \frac{\delta V^2}{2!} \left.\frac{d^2i}{dv^2}\right|_{I_0} + \cdots +$$
$$\frac{\delta V^n}{n!} \left.\frac{d^ni}{dv^n}\right|_{I_0} + \cdots \qquad . \quad (1)$$

Assuming that $\delta V = V_p\left(\cos \omega_c t\right)$ and the signal is so small that the term above the second order can be ignored, equation (1) can be simplified as follows:

$$i(V) = i(V_0) + V_p \cos\left(\omega_c t\right) \left.\frac{di}{dv}\right|_{I_0} + \frac{V_p^{\,2} \cos\left(\omega_c t\right)^2}{2} \left.\frac{d^2i}{dv^2}\right|_{I_0}$$
$$, \quad (2)$$

$$\Delta i = \frac{V_p^{\,2}}{4} \left.\frac{d^2i}{dv^2}\right|_{I_0} + V_p \cos\left(\omega_c t\right) \left.\frac{di}{dv}\right|_{I_0} +$$
$$\frac{V_p^{\,2} \cos\left(2\omega_c t\right)}{4} \left.\frac{d^2i}{dv^2}\right|_{I_0} \qquad . \quad (3)$$

Equation (3) illustrates that Δi contains the DC term, the fundamental term and the second harmonic term, and the DC term is directly proportional to the input RF power. The RF input power can be calculated by measuring the DC voltage.

The typical zero-bias detector structure is shown in Fig. 1-(a). A LPF is adopted as the RF short at the DC ground and output port, which are located at different sides of the probe. In this paper, the structure of the zero-bias detector circuit was improved based on the radial stub structure[11], as shown in Fig. 1-(b). The high and low impedance line or compact microstrip resonant cell (CMRC) LPFs, which are commonly used in detectors as the RF short end[6-9], were replaced by the radial stub, which is shorter, smaller, and helps increase the compactness of the whole circuit. Moreover, since the impedance of the radial stub is equal to zero, the DC ground and output port were connected in parallel with a radial stub structure to eliminate the influence of the external loads on the detector circuit impedance matching and bring a better stability in detector performance and conformance between measurement and simulation. Meanwhile, since the radial stub brought a large mismatch impedance, a tuning line was connected to the radial stub to modify its impedance to optimize the impedance matching and achieve a lower return loss. In addition, the DC ground and output port were placed on the same side of the probe to enable the detector circuit to be directly connected with the pre-level circuits without a waveguide-to-microstrip transition structure, which would cause more energy loss. Furthermore, this change made the detector circuit more convenient to integrate with pre-level systems and suitable for circuit integration and CubeSat radiometer miniaturization.

The High Frequency Structure Simulator (HFSS) was used in this study to design and model each passive structure separately, including the 3D electromagnetic model of the Schottky diode. The Schottky diode nonlinear model was constructed using Advanced Design System (ADS) and combined with the HFSS models to form a complete circuit model for further optimization.
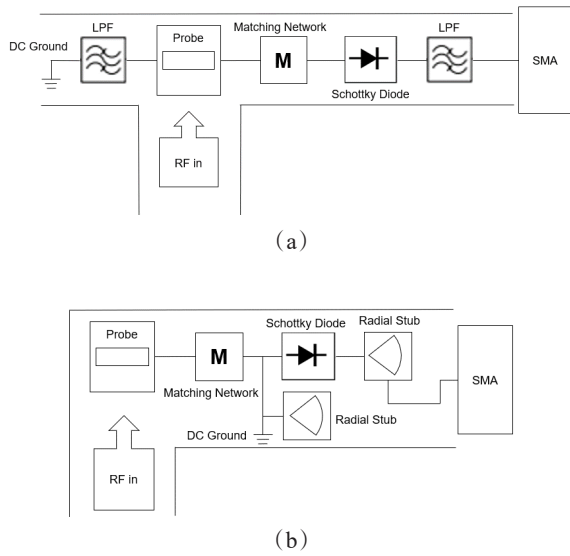
CHEN Yao *et al*:Design of millimeter-wave detectors based on zero-bias Schottky diode for direct detection system of CubeSat radiometer

1 期

287

(a)

(b)

Fig. 1　(a) Typical zero-bias detector circuit structure, (b) improved zero-bias detector structure
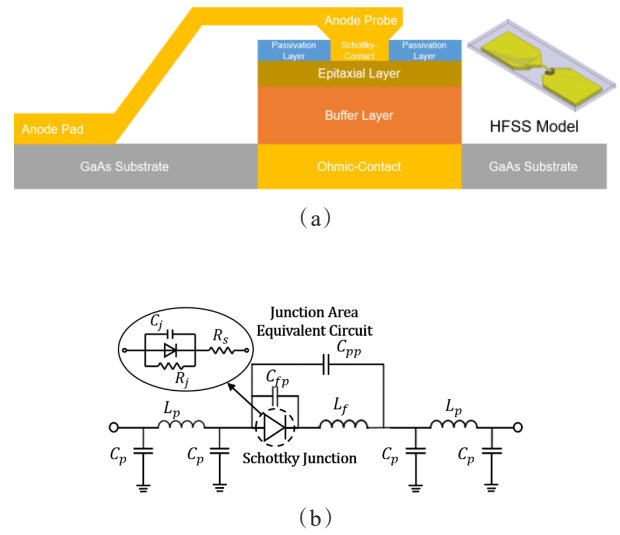图 1　(a)典型零偏置检波器电路结构,(b)改进型零偏置检波器电路结构

(a)

(b)

Fig. 2　(a) Structure of the QVSD and its 3D electromagnetic model in HFSS, (b) equivalent circuits of the QVSD and diode junction area
图 2　(a)准垂直肖特基二极管结构及其 HFSS 三维电磁模型,(b)准垂直肖特基二极管及二极管结区等效电路

1.1　Establishment of Schottky Diode Model

The detectors were designed based on the zero-bias Schottky diode of ACST used a quasi-vertical structure[12-13]. The structure of the quasi-vertical Schottky diode (QVSD) and its 3D electromagnetic model in HFSS are shown in Fig. 2(a). The diode is supported by a thin film substrate 5 μm thick and composed of an anode probe, epitaxial layer, buffer layer, and metal layer. Schottky contacts are formed on the front side of the n GaAs epitaxial layer, and ohmic contacts are formed on the back side of the n++ GaAs buffer layer, directly under the corresponding Schottky contacts. The equivalent circuits of the QVSD and diode junction area are shown in Fig. 2(b). R_j is the diode junction resistance, which can usually be ignored due to its large value. C_j is the diode junction capacitance, and R_s is the series resistance. Parasitic parameters, which are usually determined by the material and geometric structure of the diode, include the anode pad parasitic capacitance C_p, parasitic inductance L_p, air bridge inductance L_f, capacitance between the air bridge and buffer layer C_{fp}, and capacitance between the anode pad and buffer layer C_{pp}. The material and thickness of each layer of the QVSD model are listed in Table 1.

Since HFSS cannot simulate the nonlinear characteristics of the diodes, the nonlinear characteristics model needs to be established in ADS. Meanwhile, to eliminate the influence of the nonlinear structure in the HFSS model, the Schottky contacts need to be short-circuited. The short-circuit structure and the port loading model in HFSS are shown in Fig. 3(a). Its equivalent circuit is shown in Fig. 3(b).

The most important parameters of the Schottky diode nonlinear model are the junction capacitance C_j, series resistance R_s, saturation current I_s and ideal factor n. The junction capacitance C_j of 3DSF20 and 3DSF30 are 20 fF and 30 fF, respectively. The I−V characteristic of the diode can be expressed as follows:

$$I(V) = I_s \left[\exp^{\frac{qV}{nKT}} -1 \right] \quad , \quad (4)$$

where q is the electronic charge, K is the Boltzmann constant and T is the absolute temperature.

Three points, A (V_1, I_1), B (V_2, I_2), and C (V_3, I_3), were selected from the I − V characteristic curve. According to equation (4), R_s, I_s, and n can be obtained:

Table 1　3D electromagnetic model parameters of the QVSD
表 1　准垂直肖特基二极管三维电磁模型参数

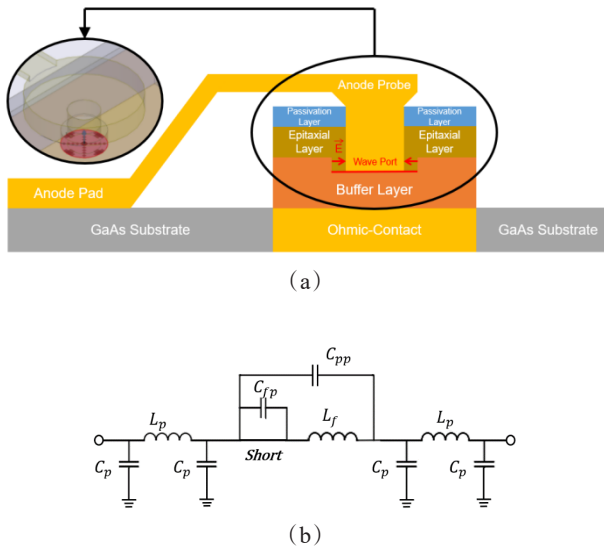| Layer	Material	Relative Dielectric Constant	Thickness (μm)
Epitaxial Layer	GaAs	12.9	0.2
Buffer Layer	Perfect Conductor	1	1.8
Thin Film Substrate	GaAs	12.9	5
Passivation Layer	SiO$_2$	4	0.5
Anode Probe & Pad	Gold	1	—

(a)

(b)

Fig. 3　(a) Short-circuit structure of the QVSD and its port loading model in HFSS (b) equivalent circuit
图 3　(a)准垂直肖特基二极管短路结构及其 HFSS 端口加载模型(b)等效电路

$$R_s = \frac{\left(V_2 - V_1\right) + \left(V_1 - V_3\right)\left(\dfrac{\ln\left(I_1/I_2\right)}{\ln\left(I_1/I_3\right)}\right)}{\left(I_2 - I_1\right) + \left(I_1 - I_3\right)\left(\dfrac{\ln\left(I_1/I_2\right)}{\ln\left(I_1/I_3\right)}\right)} \quad , \quad (5)$$

$$I_s = \frac{I_1}{\exp\left(\dfrac{V_1 - R_s I_1}{n V_t}\right) - 1} \quad , \quad (6)$$

$$n = \frac{\left(V_1 - V_2\right) + R_s\left(I_2 - I_1\right)}{V_t \ln\left(I_1/I_2\right)} \quad , \quad (7)$$

where $V_t = KT/q$ is the thermal voltage. The calculated values of the two diodes are shown in Table 2.

Table 2　Calculated R_s, I_s, and n of Schottky diodes
**表 2　肖特基二极管 Rs、Is 与 n 的计算数值**

Type	$R_s(\Omega)$	$I_s(\text{mA})$	n
3DSF20	14. 585	0. 051	1. 052
3DSF30	10. 672	0. 02	1. 059

　　While the nonlinear model of the diode can be established based on the parameters, the complete model can be obtained by combining the nonlinear model with the HFSS 3D electromagnetic model. The $I-V$ characteristic simulation results of the two Schottky diodes are shown in Fig. 4 and are basically consistent with the measured results (provided by ACST).

1. 2　Design of waveguide-to-microstrip transition
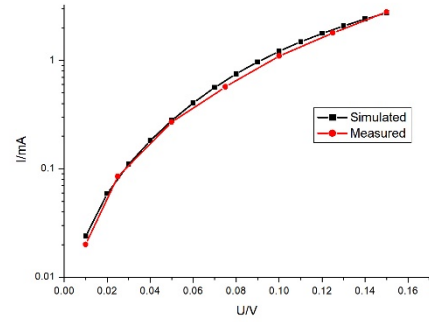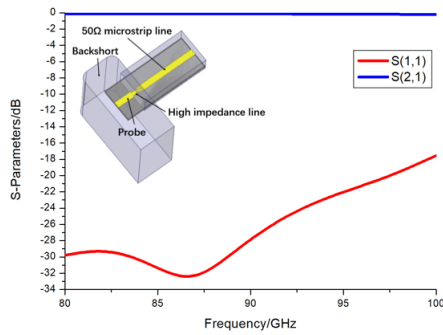

(a)
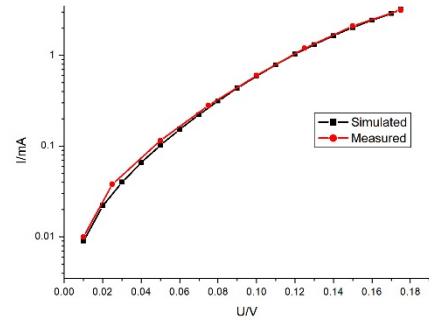
(b)

Fig. 4　Simulated and measured I-V characteristic: (a) 3DSF20 (b) 3DSF30
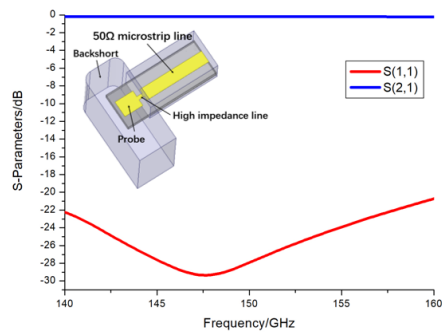图 4　伏安特性曲线仿真与测试结果：(a)3DSF20 (b)3DSF30

structure

　　There has been extensive research on developing millimeter-wave waveguide transitions using probe structures[14]. In this paper, the E-plane probe transition was adopted because of its small size and broadband low-loss performance. The transition structures were modeled and simulated in HFSS. The optimized models and simulated results are shown in Fig. 5. The insertion loss of the W-band transition model was lower than 0. 4 dB, and the return loss was better than 18 dB in the 20 GHz bandwidth. Furthermore, the insertion loss of the D-band transition model was lower than 0. 3 dB, and the return loss was better than 20 dB in the 20 GHz bandwidth.

1. 3　Design of radial stub structure

　　Generally, the radial stub structure can be equivalent to a resonant circuit composed of an inductance and capacitance[11]. By changing the radius and the central angle of the radial stub, its impedance can be adjusted to the short circuit point of the Smith chart at the input RF frequency. This means that the radial stub, which is much shorter and smaller than the LPF, can be adopted as a RF short end, and fully reflect the RF signals. In addition, since the impedance of the RF short end is approximately equal to zero, the total load impedance will be still close to zero when the load is in parallel with it.

CHEN Yao *et al*：Design of millimeter-wave detectors based on zero-bias Schottky diode for direct detection
system of CubeSat radiometer

1 期   289

(a)

(b)

Fig. 5   Transition models and simulated S-parameters: (a) W-band (b) D-band
图 5   转换结构模型及 S 参数仿真结果：(a)W 波段 (b)D 波段

Thus，the parallel branch load will not affect the total load impedance and therefore will not affect the impedance matching of the whole detector circuit. Consequently，the stability of the detector is improved. The HFSS models of the two radial stub structures used in the W-band and D-band detectors，and their Smith chart simulation results are shown in Fig. 6. It can be seen from the Smith chart simulation results that the impedances of the two radial stub structures were optimized to the short circuit point at 89 GHz and 150 GHz，respectively，and the two radial stubs can be seen as RF short ends.

1. 4   Design of matching circuit

In order to transfer as much power as possible to the diode，it is necessary to match the impedance of the diode and the two radial stub structures. The integrated circuit structure is shown in Fig. 7. Since the radial stub structures introduce a large mismatch impedance at the input RF frequency，the total load impedance at port 1 needs to be adjusted by changing the length and width of the tuning lines L_1 and L_2；this reduces the impedance matching difficulty of the integrated circuit and increases the matching bandwidth. The matching network was realized by four stepped impedance lines，and the length and width of the four matching lines were optimized to achieve the maximum energy transmission[15]. The imped-
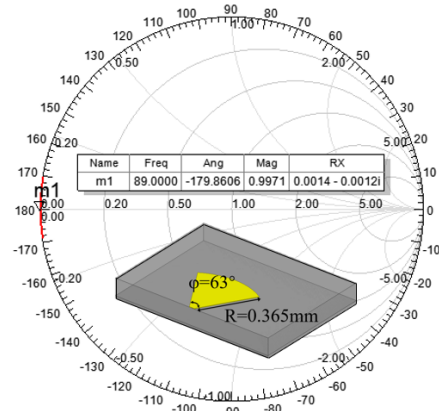
(a)
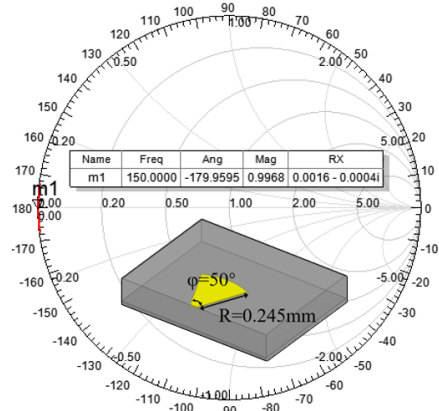
(b)

Fig. 6   Radial stub structure models and Smith chart simulation results: (a) W-band, (b) D-band
图 6   扇形线结构模型及史密斯圆图仿真结果：(a)W 波段，(b)D 波段

ance matching network and the tuning lines L_1 and L_2 were optimized in the ADS and modeled in the HFSS. The calculated parameters of L_1 and L_2 of the two detectors and their optimized normalized impedances of port 1 at 89 GHz and 150 GHz，respectively，are shown in Table 3. The integrated circuit models in HFSS are shown in Fig. 8.
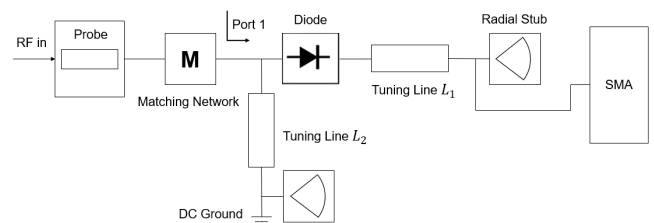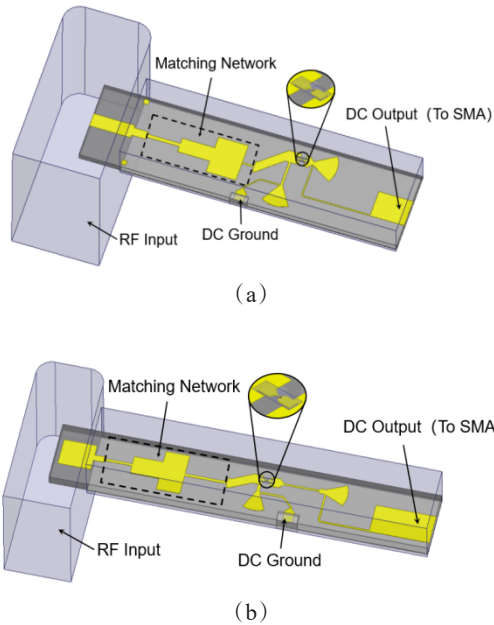

Fig. 7   Integrated circuit structure
图 7   整体电路结构

	Z_{L_1} (Ω)	θ_{L_1} (deg)	Z_{L_2} (Ω)	θ_{L_2} (deg)	Port 1 Impedance
W–band	57.24	11.03	117.89	64.73	0.611−j2.035
D–band	144.21	97.47	120.79	24.11	1.95+j1.552

(a)

(b)

Fig. 8   Integrated circuit models in HFSS: (a) W-band (b) D-band
图 8   整体电路HFSS模型：(a)W 波段 (b)D 波段

(a)

(b)

Fig. 9   Photos of two detector modules and their circuits: (a) W-band (b) D-band
图 9   两款检波器模块及其电路照片：(a)W 波段 (b)D 波段

Fig. 10   Photo of return loss test platform
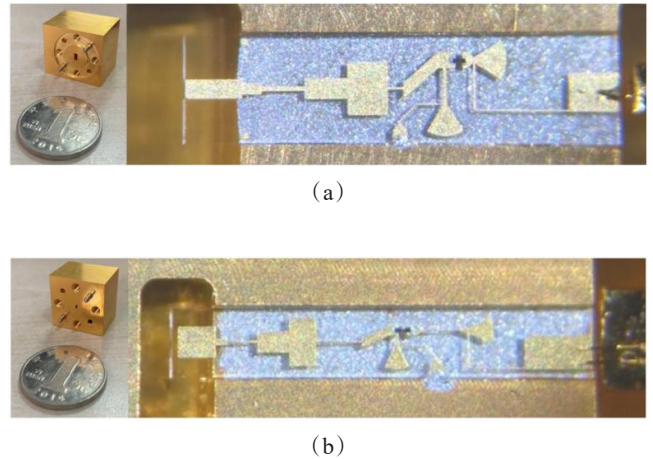图 10   回波损耗测试平台照片

2   Fabrication and measurement

2.1   Fabrication and package

The fabricated circuit was installed in the cavity. The substrate of the circuit was made of quartz glass with a relative dielectric constant of 3.78 and a thickness of 100 μm. The quartz glass circuit and DC ground were connected with the cavity through a 15 μm thick conductive adhesive. The Schottky diode was installed on the circuit through a 10 μm thick conductive adhesive. The DC output port was connected with the SMA probe through a gold bonding wire. The photos of the two detector modules and their circuits are shown in Fig. 9.

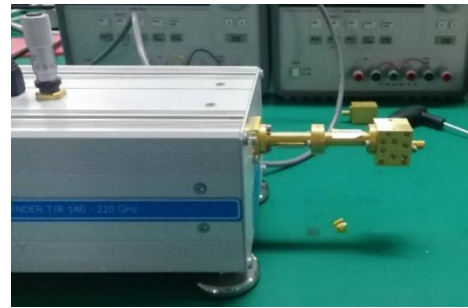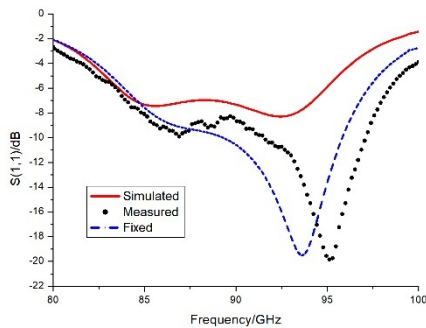### 2.2   S–Parameter measurement

The return loss of the two detectors was measured by a vector network analyzer with an extension module, as shown in Fig. 10.

The simulated, measured, and fixed return loss of the two detectors are shown in Fig. 11. The return loss of the W-band detector is better than 9 dB over the pass band and reaches 20 dB at 95 GHz. Meanwhile, the return loss of the D-band detector is better than 6 dB over the pass band. However, there are some differences between the simulated results and the measured results, es-

pecially for the W-band detector. The factors causing these differences are the fabrication deviation of the quartz circuit and the deviation of the Schottky diode itself, which mainly includes the junction capacitance deviation and series resistance deviation. The deviation of the Schottky diode has a greater influence on return loss than any other factors. Additionally, as shown in Fig. 11, the simulated results can be fixed to fit with the measured results only by changing the junction capacitance and series resistance of the Schottky diode model in a reasonable range (provided by ACST). The original and fixed parameters of the junction capacitance and series resistance of the two Schottky diodes are shown in Table 4.
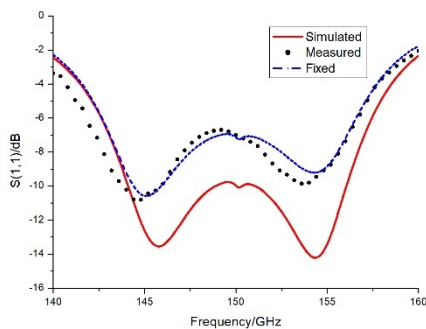
Table 4   Original and fixed parameters of C_j and R_s of the Schottky diodes

表 4   肖特基二极管Cj和Rs的初始与修正参数

Type	Parameters	Original value	Fixed value	Error range provided by ACST
3DSF20	C_j(fF)	20	21.273	16 to 24
	R_s(Ω)	14.585	10.489	—
3DSF30	C_j(fF)	30	24.627	24 to 36
	R_s(Ω)	10.725	18.986	5 to 20

CHEN Yao *et al*：Design of millimeter-wave detectors based on zero-bias Schottky diode for direct detection
system of CubeSat radiometer

1 期 291

(a)

(b)

Fig. 11　Simulated, measured, and fixed return loss: (a) W-band detector (b) D-band detector
图 11　回波损耗的仿真、测试与修正结果：(a)W 波段检波器 (b)D 波段检波器

2.3　Voltage sensitivity measurement

Voltage sensitivity reflects the ability of a detector to detect small signals and can be expressed as follow：

$$\beta_V = \frac{V_{out}}{P_{in}}, \tag{8}$$

where V_{out} is the output detection voltage and P_{in} is the input power.

A diagram of the test platform is shown in Fig. 12. The vector network analyzer was selected as the small signal source，and the signal was transmitted to the detector through the attenuator. During the test，the output power of the signal source was controlled at about -20 dBm after calibration by a power meter，and the detection voltage
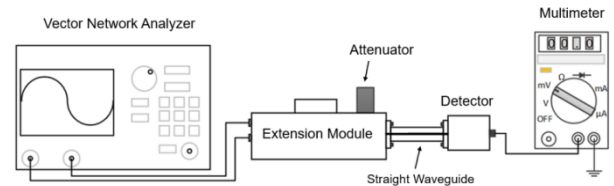
was measured by a multimeter.

Fig. 12　Test platform
图 12　测试平台

Figure 13 shows the simulated and measured voltage sensitivity of the two detectors. The typical sensitivity of the W-band detector is about 2500 V/W from 85 GHz to 95 GHz，with a maximum sensitivity of 2875 V/W at 87 GHz. Meanwhile，the typical sensitivity of the D-band detector is about 1600 V/W from 145 GHz to 155 GHz，with a maximum sensitivity of 1891 V/W at 146 GHz. Both measured results are basically consistent with the simulated results. A performance comparison of voltage sensitivity between our proposed detectors and other W-band and D-band detectors is shown in Table 5.

2.4　Linearity measurement

Linearity can measure the relationship between output voltage and input power of a detector，which directly affects the accuracy of brightness temperature measurement of a radiometer. The test platform is the same as shown in Fig. 12. The vector network analyzer was used as the small signal source，and the output power was controlled by adjusting the attenuator.

The measured linearities of the two detectors are shown in Fig. 14. The linearity was measured at 89 GHz and 150 GHz for the W-band detector and D-band detector，respectively. When the input power is in the range of 5 μW to 40 μW，the linearity of the W-band detector is about 0.9994. Meanwhile，when the input power is in the range of 3 μW to 18 μW，the linearity of the D-band detector is about 0.9992.

3　Conclusion

Two millimeter-wave detectors with an improved circuit structure were designed and implemented in this paper. The improved circuit structure based on the radial stub is more stable and compact compared to the typical circuit structure. The W-band detector has a typical sensitivity about 2500 V/W in the range of 85 GHz to 95 GHz，and a linearity of 0.9994 at 89 GHz. Meanwhile，the D-band detector has a typical sensitivity about 1600

Table 5　Voltage sensitivity comparison
表 5　电压灵敏度比较

Ref.	W−band Frequency/GHz	Voltage Sensitivity（V/W）	D−band Frequency/GHz	Voltage Sensitivity（V/W）
[5]	79~93	>860	—	—
[6]	85~110	Typ 750, MAX 1000	—	—
[8]	86~94	>2000	—	—
[9]	80~104	>2000	120~155	Typ 600, MAX 1600
This work	85~95	Typ 2500, MAX 2875	145~155	Typ 1600, MAX 1891
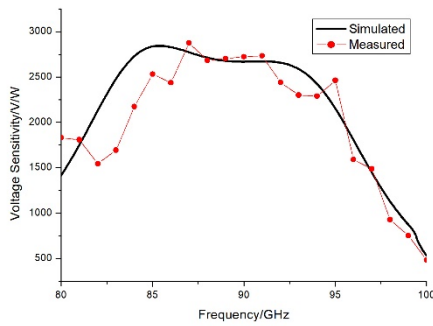
(a)
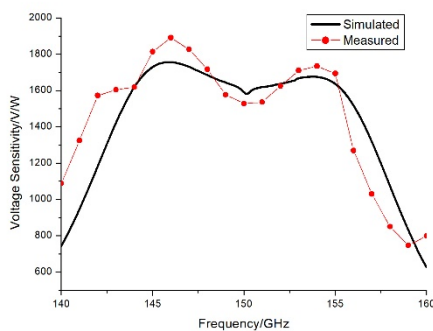
(b)

Fig. 13　Simulated and measured voltage sensitivity: (a) W-band detector (b) D-band detector

图 13　电压灵敏度仿真与测试结果：(a)W 波段检波器 (b)D 波段检波器

(a)

(b)

Fig. 14　Measured linearity: (a) W-band detector, (b) D-band detector

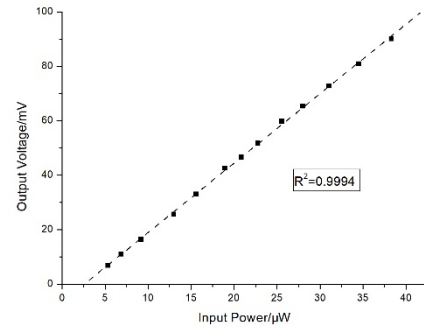图 14　线性度测试结果：(a)W 波段检波器，(b)D 波段检波器

V/W in the range of 145 GHz to 155 GHz，and a linearity of 0. 9992 at 150 GHz. The measured results are basically consistent with the simulated results. The fabricated detectors using the improved circuit structure based on the radial stub and tuning lines achieved broadband high voltage sensitivity，accurate in-band return loss，and high in-band linearity. And benefit from changing the DC ground port's position，it is easier to realize broadband characteristics and integrate with pre-level systems of the CubeSat radiometer direct detection channels without using waveguide-microstrip transition structures，which would result in more energy loss. Our results verify that the detectors with the improved circuit structure can meet the technical requirements of the direct detection system，and are more suitable for CubeSat applications compared to typical detectors.
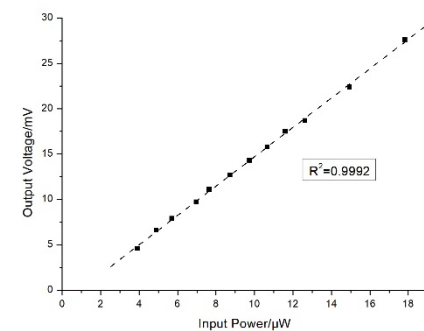
Acknowledgment

We thank LetPub (www. letpub. com) for its linguistic assistance during the preparation of this manuscript.

References

［1］Reising S C , Gaier T C , Brown S T , et al. Temporal Experiment for Storms and Tropical Systems Technology Demonstration (TEMPEST-D) 6U CubeSat Mission：Early Results and Potential for Atmospheric Science［C］. 2019 URSI Asia-Pacific Radio Science Conference (AP-RASC), New Delhi, India, 2019.

［2］Padmanabhan S , Gaier T C , Tanner A B , et al. TEMPEST-D Radiometer：Instrument Description and Prelaunch Calibration ［J］. IEEE Transactions on Geoscience and Remote Sensing, 2020：1-14.

［3］B. Lim, S. Statham, S. Misra, J. et al. The Radiometer Atmospheric CubeSat Experiment (RACE) pre-launch performance ［C］. 2015 IEEE MTT-S International Microwave Symposium, Phoenix, AZ, 2015.

［4］K. Cahoy, et al. Development of the Microwave Radiometer Technology Acceleration (MiRaTA) CubeSat for all-weather atmospheric sounding［C］. 2015 IEEE International Geoscience and Remote Sensing Symposium (IGARSS), Milan, 2015.

［5］M. Hoefle, A. Penirschke, O. Cojocari, et al. 89 GHz zero-bias Schottky detector for direct detection radiometry in European satellite programme MetOp-SG ［J］. Electronics Letters, 2014, 50 (8)：606-608.

［6］M. Tekbaş, M. S. Erdoğan, İ. Ünal. A W band waveguide detector module using zero bias schowttky diode［C］. 2017 IEEE 37th International Conference on Electronics and Nanotechnology (ELNANO), Kiev, 2017.

［7］ZHANG Jian-Jun, ZHOU Jing-Tao, YANG Cheng-Yue, et al. A 270 GHz high performance waveguide detector utilizing a zero-bias Schottky diode［J］. J.Infrared Millim. Waves（张建军，周静涛，杨成樾，等. 基于零偏置肖特基二极管的270GHz高性能波导检波器. 红外与毫米波学报），2015, 34(1)：1-5.

［8］W. Zhang, F. Yang, Z. X. Wang. W-band(90GHz) zero bias Schottky diode directive detector［C］. 2015 Asia-Pacific Microwave Conference (APMC), Nanjing, 2015.

CHEN Yao *et al*：Design of millimeter-wave detectors based on zero-bias Schottky diode for direct detection
system of CubeSat radiometer

1 期　　293

［9］YAO Chang-Fei，ZHOU Ming，LUO Yun-Sheng，*et al*. Millimeter wave broadband high sensitivity detectors with zero-bias Schottky diodes［J］. *Journal of Semiconductors*，2015，**36**（6）：109-113.

［10］DB/OL］：https：//www.acst.com.

［11］F. Giannini，C. Paoloni. Broadband lumped equivalent circuit for shunt-connected radial stub［J］. *Electronics Letters*，1986，**22**（9）：485 - 487.

［12］M. Hoefle，K. Schneider，A. Penirschke，*et al*. Characterization and impedance matching of new high sensitive planar Schottky detector diodes［C］. 2011 German Microwave Conference，Darmstadt，2011.

［13］O. Cojocari，C. Sydlo，H. Hartnagel，*et al*. Schottky-Structures for THz-Applications based on Quasi-Vertical Design-Concept［C］. Sixteenth International Symposium on Space Terahertz Technology，2005.

［14］Xiaoxing Ma，Ruimin Xu. A broadband W-band E-plan waveguide-to-microstrip probe transition［C］. 2008 Asia-Pacific Microwave Conference，Macau，2008.

［15］A. G. Radwan，A. Shamim，K. N. Salama. Theory of Fractional Order Elements Based Impedance Matching Networks［J］. *IEEE Microwave and Wireless Components Letters*，2011，**21**（3）：120-122.